

# PU-Transformer: Point Cloud Upsampling Transformer

Shi Qiu<sup>1,2</sup>, Saeed Anwar<sup>1,2</sup> and Nick Barnes<sup>1</sup>

<sup>1</sup>Australian National University, <sup>2</sup>Data61-CSIRO, Australia

{shi.qiu, saeed.anwar, nick.barnes}@anu.edu.au

## Abstract

Given the rapid development of 3D scanners, point clouds are becoming popular in AI-driven machines. However, point cloud data is inherently sparse and irregular, causing major difficulties for machine perception. In this work, we focus on the point cloud upsampling task that intends to generate dense high-fidelity point clouds from sparse input data. Specifically, to activate the transformer’s strong capability in representing features, we develop a new variant of a multi-head self-attention structure to enhance both point-wise and channel-wise relations of the feature map. In addition, we leverage a positional fusion block to comprehensively capture the local context of point cloud data, providing more position-related information about the scattered points. As the first transformer model introduced for point cloud upsampling, we demonstrate the outstanding performance of our approach by comparing with the state-of-the-art CNN-based methods on different benchmarks quantitatively and qualitatively.

## 1. Introduction

3D computer vision has been attracting a wide range of interest from academia and industry since it shows great potential in many fast-developing AI-related applications such as robotics, autonomous driving, augmented reality, etc. As a basic representation of 3D data, point clouds can be easily captured by 3D sensors [15, 22], incorporating the rich context of real-world surroundings.

Unlike well-structured 2D images, point cloud data has inherent properties of *irregularity* and *sparsity*, posing enormous challenges for high-level vision tasks such as point cloud classification [39, 55, 44], segmentation [40, 43, 19], and object detection [38, 37, 47]. For instance, Uy *et al.* [51] fail to predict the real-world point clouds’ labels when they apply a model that was pre-trained using synthetic data; and the segmentation [19, 46] and detection [36] results on distant/smaller point cloud objects (*e.g.*, bicycles, traffic-signs) are worse than the closer/larger objects (*e.g.*, vehicles, buildings) captured by LiDAR scanners [5, 7]. If we

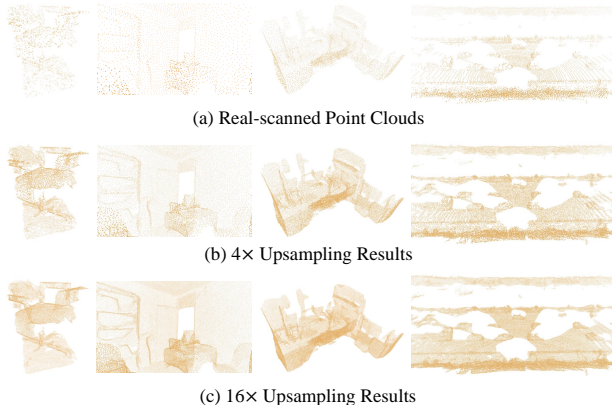


Figure 1: Examples of upsampling real scanned point clouds using PU-Transformer. The first column presents a “chair” [51], while the others illustrate scenes of an “office” [3], a “room” [12] and a “street” [5], respectively. Given sparse point clouds, the dense outputs of PU-Transformer have uniform point distributions showing high-fidelity details. Particularly, the contours of upsampled object instances (*e.g.*, tables in “office/room”, cars in “street”) are clearly distinct from the complex surroundings, benefiting further visual analysis.

tackle the data’s *irregularity* and *sparsity*, further improvements in point cloud analysis can be obtained. To this end, the point cloud upsampling task is worthy of investigation.

As a basic 3D low-level vision task, point cloud upsampling aims to generate dense point clouds from sparse input, where the generated data should recover the fine-grained structures at a higher resolution. Moreover, the upsampled points are expected to lie on the underlying surfaces in a uniform distribution, benefiting downstream tasks for both 3D visual analysis [30, 45] and graphic modeling [34, 33]. Following the success of Convolution Neural Networks (CNNs) in image super-resolution [13, 25, 2] and Multi-Layer-Perceptrons (MLPs) in point cloud analysis [39, 40], previous point cloud upsampling networks [58, 57, 28, 42, 41, 29] developed MLP-based structures to encode features and estimate new points. Although such an MLP operation can learn from point cloud data, the effectiveness of a whole network is limited by the MLP’s insufficient expression and generalization capability. Differ-

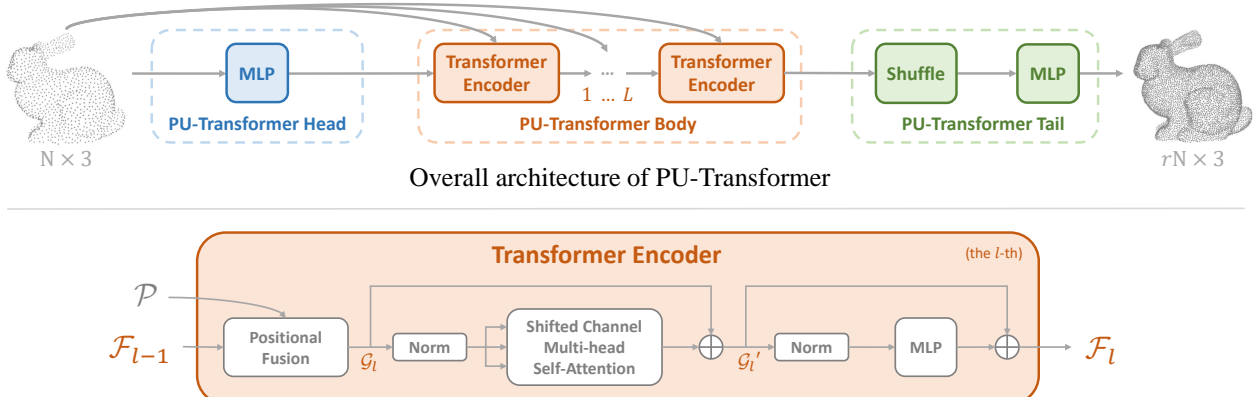


Figure 2: The details of PU-Transformer. The upper chart shows the overall architecture of the PU-Transformer model containing three main parts: the PU-Transformer head (Sec. 4.1), body (Sec. 4.2), and tail (Sec. 4.3). The PU-Transformer body includes a cascaded set of Transformer Encoders, serving as the core component of the whole PU-Transformer model. Particularly, the detailed structure of each Transformer Encoder (e.g., the PU-Transformer body contains  $L$  Transformer Encoders in total) is illustrated in the lower chart, where all annotations are consistent with Line 3-5 in Alg. 1.

ent from existing methods, we introduce a powerful transformer model named PU-Transformer, specializing in the point cloud upsampling task. Next, we explain our key reasons for adopting transformers to point cloud upsampling.

*Plausibility in theory.* As the core operation of transformers, self-attention [52] is a set operator [61] calculating long-range dependencies between elements regardless of data order. On this front, self-attention can perfectly suit the point cloud data and easily estimate the point-wise dependencies without any concern for the inherent *unorderedness*. Moreover, to represent a comprehensive feature map for point cloud analysis, channel-wise information also has been shown to be a crucial factor in attention mechanisms [44, 47]. Based on these facts, we propose a novel Shifted Channel Multi-head Self-Attention (SC-MSA) block, which strengthens the point-wise relations in a multi-head form and enhances the channel-wise connections by introducing the overlapping channels between consecutive heads.

*Feasibility in practice.* Since the transformer model was originally invented for natural language processing; its usage has been widely recognized in high-level visual applications for 2D images [8, 14, 31]. More recently, Chen *et al.* [10] introduced a pre-trained transformer model achieving excellent performance on image super-resolution and denoising. Inspired by the transformer’s effectiveness for image-related low-level vision tasks, we attempt to create a transformer-based model for point cloud upsampling. Given the mentioned differences between 2D images and 3D point clouds, we introduce the Positional Fusion block as a replacement for positional encoding in conventional transformers: on the one hand, local information is aggregated from both the *geometric* and *feature* context of the points, implying their 3D positional relations; on the other

hand, such *local* information can serve as complementary to subsequent self-attention operations, where the point-wise dependencies are calculated from a *global* perspective.

*Adaptability in various applications.* Transformer-based models are considered as a luxury tool in computer vision due to the huge consumption of data, hardware, and computational resources. However, our PU-Transformer can be easily trained with a *single* standard GPU (e.g., GeForce 1080/2080 Ti) in a few hours, retaining a similar model complexity to regular CNN-based point cloud upsampling networks [58, 57, 29]. Moreover, following a patch-based pipeline [57], the trained PU-Transformer model can effectively and flexibly upsample different types of point cloud data, including but not limited to regular object instances or large-scale LiDAR scenes as shown in Fig. 1. Starting with the fundamental upsampling task in low-level vision, we expect our approach to transformers will be affordable in terms of resource consumption for most researchers, further extending the applications of point clouds.

Our main contributions are in these aspects:

- To the best of our knowledge, we are the first to introduce a transformer-based model for point cloud upsampling. The whole project of our PU-Transformer will be released<sup>1</sup> to the public.
- We quantitatively validate the effectiveness of the PU-Transformer by significantly outperforming the results of state-of-the-art point cloud upsampling networks on two benchmarks using three metrics.
- The upsampled visualizations demonstrate the superiority of PU-Transformer for diverse point clouds.

<sup>1</sup>The source code and trained models will be available at: <https://github.com/>.

## 2. Related Work

**Point Cloud Networks:** In early research, the projection-based methods [50, 26] used to project 3D point clouds into multi-view 2D images, apply regular 2D convolutions for feature extraction, and finally fuse the extracted information for 3D analysis. Alternatively, discretization-based approaches [18] tended to convert the point clouds to voxels [20] or lattices [49], and then process them using 3D convolutions or sparse tensor convolutions [11]. To avoid context loss and complex steps during data conversion, the point-based networks [39, 40, 55] directly process point cloud data via MLP-based operations. Although current mainstream approaches in point cloud upsampling prefer utilizing MLP-related modules, in this paper, we focus on an advanced transformer structure [52] in order to further enhance the point-wise dependencies between known points and benefit the generation of new points.

**Point Cloud Upsampling:** Despite the fact that current point cloud research in low-level vision [58, 60] is less active than that in high-level analysis [39, 19, 38], there exist many outstanding works that have contributed significant developments to the point cloud upsampling task. To be specific, PU-Net [58] is a pioneering work that introduced CNNs to point cloud upsampling based on a PointNet++ [40] like backbone. Later, MPU [57] proposed a patch-based upsampling pipeline, which can flexibly upsample the point cloud patches with rich local details. In addition, PU-GAN [28] adopted the architecture of Generative Adversarial Networks [16] for the generation problem of high-resolution point clouds, while PUGeo-Net [42] indicated a promising combination of discrete differential geometry and deep learning. More recently, Dis-PU [29] applies disentangled refinement units to gradually generate the high-quality point clouds from coarse ones, and PU-GCN [41] achieves good upsampling performance by using graph-based constructions [55] in the network. As the first work that leverages the powerful transformer structure for point cloud upsampling, we hope that our PU-Transformer attracts more research interest and inspires future work in relevant topics.

**Transformers in Vision:** With the capacity in parallel processing as well as the scalability to deep networks and large datasets [24], an increasing number of visual transformers have achieved excellent performance on image-related tasks including either low-level super-resolution [56, 10] or high-level classification [14, 31], detection [8, 62]. Due to the inherent gaps between 3D and 2D data, transformer-based approaches to point cloud analysis have not been fully developed. In terms of regular point cloud classification and segmentation, researchers introduce some variants of transformer using vector-attention [61], offset-attention [17], and grid-rasterization [32], etc. However, since these trans-

---

### Algorithm 1: PU-Transformer Pipeline

---

```

input: a sparse point cloud  $\mathcal{P} \in \mathbb{R}^{N \times 3}$ 
output: a dense point cloud  $\mathcal{S} \in \mathbb{R}^{rN \times 3}$ 
# PU-Transformer Head
1  $\mathcal{F}_0 = \text{MLP}(\mathcal{P})$ 
# PU-Transformer Body
2 for each Transformer Encoder do
    #  $l = 1 \dots L$ 
    # the  $l$ -th Transformer Encoder
3    $\mathcal{G}_l = \text{PosFus}(\mathcal{P}, \mathcal{F}_{l-1})$ ;
4    $\mathcal{G}_l' = \text{SC-MSA}(\text{Norm}(\mathcal{G}_l)) + \mathcal{G}_l$ ;
5    $\mathcal{F}_l = \text{MLP}(\text{Norm}(\mathcal{G}_l')) + \mathcal{G}_l'$ ;
6 end for
# PU-Transformer Tail
7  $\mathcal{S} = \text{MLP}(\text{Shuffle}(\mathcal{F}_L))$ 

```

---

formers still operate on an overall classical PointNet [39] or PointNet++ architecture [40], the improvement is relatively limited while the computational cost is too expensive for most researchers to re-implement. In contrast, recent PoinTr [59] shows great effectiveness in point cloud completion by adopting the standard architecture of transformer models [52], which consists of both the transformer encoders and decoders. To simplify the model’s complexity and boost its adaptability in point cloud upsampling research, we only utilize the general structure of transformer encoder [14] to form the body of our PU-Transformer.

## 3. Methodology

### 3.1. Overview

As shown in Fig. 2, given a sparse point cloud  $\mathcal{P} \in \mathbb{R}^{N \times 3}$ , our proposed PU-Transformer can generate a dense point cloud  $\mathcal{S} \in \mathbb{R}^{rN \times 3}$ , where  $r$  denotes the upsampling scale. Firstly, the PU-Transformer head extracts a preliminary feature map from the input. Then, based on the extracted feature map and the inherent 3D coordinates, the PU-Transformer body gradually encodes a more comprehensive feature map via the cascaded Transformer Encoders. Finally, in the PU-Transformer tail, we use the shuffle operation [48] to form a dense feature map and reconstruct the 3D coordinates of  $\mathcal{S}$  via an MLP.

In Alg. 1, we present the basic operations that are employed to build our PU-Transformer. As well as the operations (“MLP” [39], “Norm” [4], “Shuffle” [48]) that have been widely used in image and point cloud analysis, we propose two novel blocks targeting a transformer-based point cloud upsampling model *i.e.*, the Positional Fusion block (“PosFus” in Alg. 1), and the Shifted-Channel Multi-head Self-Attention block (“SC-MSA” in Alg. 1). In the rest of this section, we introduce these two blocks in detail. Moreover, for a compact description, we only consider the case of an *arbitrary* Transformer Encoder; thus, in the follow-

ing, we discard the subscripts that are annotated in Alg. 1 denoting a Transformer Encoder’s specific index in the PU-Transformer body.

### 3.2. Positional Fusion

Usually, a point cloud consisting of  $N$  points has two main types of context: the 3D coordinates  $\mathcal{P} \in \mathbb{R}^{N \times 3}$  that are explicitly sampled from synthetic meshes or captured by real-world scanners, showing the original geometric distribution of the points in 3D space; and the feature context,  $\mathcal{F} \in \mathbb{R}^{N \times C}$ , that is implicitly encoded by convolutional operations in  $C$ -dimensional embedding space, yielding rich latent clues for visual analysis. Older approaches [58, 57, 28] to point cloud upsampling generate a dense point set by heavily exploiting the encoded features  $\mathcal{F}$ , while recent methods [42, 41] attempt to incorporate more geometric information. As the core module of the PU-Transformer, the proposed Transformer Encoder leverages a Positional Fusion block to encode and combine both the given  $\mathcal{P}$  and  $\mathcal{F}$ <sup>2</sup> of a point cloud, following the local geometric relations between the scattered points.

Based on the metric of *3D-Euclidean distance*, we can search for neighbors  $\forall p_j \in Ni(p_i)$  for each point  $p_i \in \mathbb{R}^3$  in the given point cloud  $\mathcal{P}$ , using the k-nearest-neighbors (knn) algorithm [55]. Coupled with a grouping operation, we thus obtain a matrix  $\mathcal{P}_j \in \mathbb{R}^{N \times k \times 3}$ , denoting the 3D coordinates of the neighbors for all points. Accordingly, the relative positions between each point and its neighbors can be formulated as:

$$\Delta\mathcal{P} = \mathcal{P}_j - \mathcal{P}, \quad \Delta\mathcal{P} \in \mathbb{R}^{N \times k \times 3}; \quad (1)$$

where  $k$  is the number of neighbors. In addition to the neighbors’ relative positions showing each point’s local detail, we also append the centroids’ absolute positions in 3D space, indicating the global distribution for all points. By duplicating  $\mathcal{P}$  in a dimension expanded  $k$  times, we concatenate the local *geometric* context as:

$$\mathcal{G}_{geo} = \text{concat} \left[ \text{dup}(\mathcal{P}); \Delta\mathcal{P} \right] \in \mathbb{R}^{N \times k \times 6}. \quad (2)$$

Further, for the feature matrix  $\mathcal{F}_j \in \mathbb{R}^{N \times k \times C}$  of all searched neighbors, we conduct similar operations (Eq. 1 and 2) as on the counterpart  $\mathcal{P}_j$ , computing the relative features as:

$$\Delta\mathcal{F} = \mathcal{F}_j - \mathcal{F}, \quad \Delta\mathcal{F} \in \mathbb{R}^{N \times k \times C}; \quad (3)$$

and representing the local *feature* context as:

$$\mathcal{G}_{feat} = \text{concat} \left[ \text{dup}(\mathcal{F}); \Delta\mathcal{F} \right] \in \mathbb{R}^{N \times k \times 2C}. \quad (4)$$

<sup>2</sup>equivalent to “ $\mathcal{F}_{l-1}$ ” in Alg. 1

After the local *geometric* context  $\mathcal{G}_{geo}$  and local *feature* context  $\mathcal{G}_{feat}$  are constructed, we then fuse them for a comprehensive point feature representation. Specifically,  $\mathcal{G}_{geo}$  and  $\mathcal{G}_{feat}$  are encoded via two MLPs,  $\mathcal{M}_\Phi$  and  $\mathcal{M}_\Theta$ , respectively; further, we comprehensively aggregate the local information,  $\mathcal{G} \in \mathbb{R}^{N \times C^3}$ , using a concatenation between the encoded two types of local context, followed by a max-pooling function operating over the neighborhoods. The above operations can be summarized as:

$$\mathcal{G} = \max_k \left( \text{concat} \left[ \mathcal{M}_\Phi(\mathcal{G}_{geo}); \mathcal{M}_\Theta(\mathcal{G}_{feat}) \right] \right). \quad (5)$$

Unlike the local graphs in DGCNN [55] that need to be updated in every encoder based on the *dynamic* relations in embedding space, both of our  $\mathcal{G}_{geo}$  and  $\mathcal{G}_{feat}$  are constructed (*i.e.*, Eq. 2 and 4) and encoded (*i.e.*,  $\mathcal{M}_\Phi$  and  $\mathcal{M}_\Theta$  in Eq. 5) in the same way, following *fixed* 3D geometric relations (*i.e.*,  $\forall p_j \in Ni(p_i)$  defined upon *3D-Euclidean distance*). The main benefits of our approach can be concluded from two aspects: (i) it is practically efficient since the expensive knn algorithm just needs to be conducted once, while the searching results can be utilized in all Positional Encoding blocks of the PU-Transformer body; and (ii) the local *geometric* and *feature* context are represented in a similar manner following the same metric, contributing to *fairly fusing* the two types of context.

Overall, the Positional Fusion block can not only encode the positional information about a set of unordered points for the transformer’s processing, but also aggregate comprehensive local details for accurate point cloud upsampling.

### 3.3. Shifted Channel Multi-head Self-Attention

Compared to regular self-attention [52], multi-head self-attention (MSA) [52] can capture more information by conducting the self-attention calculation in multiple heads, and thus has been widely utilized as the main calculation block in most transformer models. However, the element-wise (*i.e.*, point-wise *w.r.t.* point cloud data) dependencies in each head are independently estimated by calculating the dot-products of feature vectors, leading to a lack of connection between the outputs of different heads. To tackle this issue, we introduce a novel Shifted Channel Multi-head Self-Attention (SC-MSA) block for PU-Transformer.

As Alg. 2 states, at first, we apply linear layers (denoted as “Linear”, and implement as a  $1 \times 1$  convolution) to encode the query matrix  $\mathcal{Q}$ , key matrix  $\mathcal{K}$ , and value matrix  $\mathcal{V}$ . Then, we generate low-dimensional splits of  $\mathcal{Q}_m, \mathcal{K}_m, \mathcal{V}_m$  for each head. Particularly, as shown in Fig. 3, regular MSA generates the *independent* splits for the self-attention calculation in corresponding heads. In contrast, our SC-MSA applies a window (dashed square) shift along the channels to ensure that any two consecutive splits have an overlap

<sup>3</sup>equivalent to “ $\mathcal{G}_l$ ” in Alg. 1

---

**Algorithm 2:** Shifted Channel Multi-head Self-Attention (SC-MSA) Implementation

---

**input:** a point cloud feature map:  $\mathcal{I} \in \mathbb{R}^{N \times C'}$   
**output:** the refined feature map:  $\mathcal{O} \in \mathbb{R}^{N \times C'}$   
**others:** channel-wise split width:  $w$   
channel-wise shift interval:  $d, d < w$   
the number of heads:  $M$

- 1  $\mathcal{Q} = \text{Linear}(\mathcal{I})$  # Query Mat  $\mathcal{Q} \in \mathbb{R}^{N \times C'}$
- 2  $\mathcal{K} = \text{Linear}(\mathcal{I})$  # Key Mat  $\mathcal{K} \in \mathbb{R}^{N \times C'}$
- 3  $\mathcal{V} = \text{Linear}(\mathcal{I})$  # Value Mat  $\mathcal{V} \in \mathbb{R}^{N \times C'}$
- 4 **for**  $m \in \{1, 2, \dots, M\}$  **do**
- 5    $\mathcal{Q}_m = \mathcal{Q}[:, (m-1)d : (m-1)d + w];$
- 6    $\mathcal{K}_m = \mathcal{K}[:, (m-1)d : (m-1)d + w];$
- 7    $\mathcal{V}_m = \mathcal{V}[:, (m-1)d : (m-1)d + w];$
- 8    $\mathcal{A}_m = \text{softmax}(\mathcal{Q}_m \mathcal{K}_m^T);$
- 9    $\mathcal{O}_m = \mathcal{A}_m \mathcal{V}_m;$
- 10 **end for**
- 11 **obtain:**  $\{\mathcal{O}_1, \mathcal{O}_2, \dots, \mathcal{O}_M\}$
- 12  $\mathcal{O} = \text{Linear}(\text{concat}[\{\mathcal{O}_1, \mathcal{O}_2, \dots, \mathcal{O}_M\}])$

---

of  $(w - d)$  channels (slashed area), where  $w$  is the channel dimension of each split and  $d$  represents the channel-wise shift interval each time. After generating the  $\mathcal{Q}_m, \mathcal{K}_m, \mathcal{V}_m$  for each head in the mentioned manner, we employ self-attention (Alg. 2 steps 8-9) to estimate the point-wise dependencies as the output  $\mathcal{O}_m$  of each head. Considering the fact that any two consecutive heads have part of the input in common (*i.e.*, the overlap channels), thus the connections between the outputs  $\{\mathcal{O}_1, \mathcal{O}_2, \dots, \mathcal{O}_M\}$  (Alg. 2 step 11) of multiple heads are established. There are two major benefits of such connections: (i) it is easier to integrate the information between the *connected* multi-head outputs (Alg. 2 step 12), compared to using the *independent* multi-head results of regular MSA; and (ii) as the overlapping context is captured from the channel dimension, our SC-MSA can further enhance the channel-wise relations in the final output  $\mathcal{O}$ , while regular MSA only focuses on point-wise information.

It is worth noting that SC-MSA requires the shift interval to be smaller than the channel-wise width of each split (*i.e.*,  $d < w$  as in Alg. 2) for a shared area between any two consecutive splits. Accordingly, the number of heads in our SC-MSA is higher than regular MSA (*i.e.*,  $M > C'/w$  in Fig. 3). More implementation detail and the choices of shift-related parameters are provided in Sec. 4.2.

## 4. Implementation

### 4.1. PU-Transformer Head

As illustrated in Fig. 2, our PU-Transformer model begins with the PU-Transformer head to encode a preliminary feature map for the following operations. In practice, we only use a single layer MLP (*i.e.*, a single  $1 \times 1$  convo-

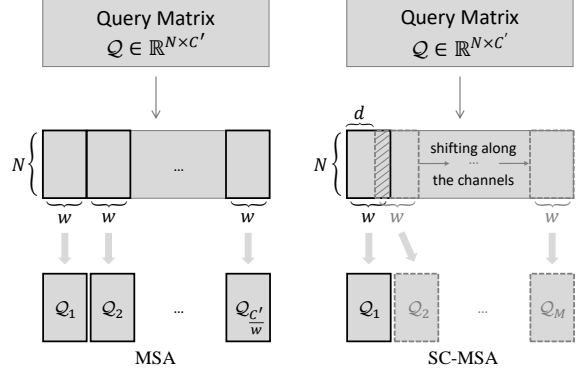


Figure 3: Examples of how regular MSA [52] and our SC-MSA generate the low-dimensional splits of query matrix  $\mathcal{Q}$  for multi-head processing (the same procedure also applies to  $\mathcal{K}$  and  $\mathcal{V}$ ).

lution, followed by a batch normalization layer [21] and a ReLU activation [35]) as the PU-Transformer head, where the generated feature map size is  $N \times 16$ .

### 4.2. PU-Transformer Body

To balance the model complexity and effectiveness, empirically, we leverage *five* cascaded Transformer Encoders (*i.e.*,  $L = 5$  in Alg. 1 and Fig. 2) to form the PU-Transformer body, where the channel dimension of each output follows:  $32 \rightarrow 64 \rightarrow 128 \rightarrow 256 \rightarrow 256$ . Particularly, in each Transformer Encoder, we only use the Positional Fusion block to encode the corresponding channel dimension (*i.e.*,  $C'$  in Eq. 5), which remains the same in the subsequent operations. For all Positional Fusion blocks, the number of neighbors is empirically set to  $k = 20$  as used in previous works [55, 41].

In terms of the SC-MSA block, the primary way of choosing the shift-related parameters is inspired by the Non-local Network [54] and ECA-Net [53]. Specifically, a reduction ratio  $\psi$  [54] is introduced to generate the low-dimensional matrices in self-attention; following a similar method, the channel-wise width (*i.e.*, channel dimension) of each split in SC-MSA is set as  $w = C'/\psi$ . Moreover, since the channel dimension is usually set to a power of 2 [53], we simply set the channel-wise shift interval  $d = w/2$ . Therefore, the number of heads in SC-MSA becomes  $M = 2\psi - 1$ . In our implementation,  $\psi = 4$  is adopted in all SC-MSA blocks of PU-Transformer.

### 4.3. PU-Transformer Tail

Based on the practical settings mentioned above, the input to the PU-Transformer tail (*i.e.*, the output of the last Transformer Encoder) has a size of  $N \times 256$ . Then, following a similar approach to pixel shuffle [48], we reform it into a dense feature map of  $rN \times 256/r$ , where  $r$  is the up-sampling scale. Finally, another MLP is utilized to estimate the upsampled point cloud's 3D coordinates ( $rN \times 3$ ).

Table 1: Quantitative comparisons to state-of-the-art methods on the *PU1K* dataset [41]. The best results are denoted in **bold**.

| Methods     | <i>Chamfer Distance</i>          | <i>Hausdorff Distance</i>        | <i>Point-to-Surface Distance</i>  |
|-------------|----------------------------------|----------------------------------|-----------------------------------|
|             | $CD \downarrow (\times 10^{-3})$ | $HD \downarrow (\times 10^{-3})$ | $P2F \downarrow (\times 10^{-3})$ |
| PU-Net [58] | 1.155                            | 15.170                           | 4.834                             |
| MPU [57]    | 0.935                            | 13.327                           | 3.551                             |
| PU-GCN [41] | 0.585                            | 7.577                            | 2.499                             |
| <b>Ours</b> | <b>0.451</b>                     | <b>3.843</b>                     | <b>1.277</b>                      |

## 5. Experiments

### 5.1. Settings

**Training Details:** In general, our PU-Transformer is implemented using Tensorflow [1] with a single GeForce 2080 Ti GPU running on the Linux OS. In terms of the hyperparameters for training, we heavily adopt the settings from PU-GCN [41] and Dis-PU [29] for the experiments in Tab. 1 and Tab. 2, respectively. For example, we have a batch size of 64 for 100 training epochs, an initial learning rate of  $1 \times 10^{-3}$  with a 0.7 decay rate, *etc*. Moreover, we only use the modified Chamfer Distance loss [57] to train the PU-Transformer, minimizing the average closest point distance between the input set  $\mathcal{P} \in \mathbb{R}^{N \times 3}$  and the output set  $\mathcal{S} \in \mathbb{R}^{rN \times 3}$  for efficient and effective convergence.

**Datasets:** To quantitatively evaluate the PU-Transformer’s effectiveness on point cloud upsampling, we train and test our proposed model using two 3D benchmarks.

- **PU1K:** This is a new point cloud upsampling dataset introduced in PU-GCN [41]. In general, the PU1K dataset incorporates 1,020 3D meshes for training and 127 3D meshes for testing, where most 3D meshes are collected from ShapeNetCore [9] covering 50 object categories. To fit in with the patch-based upsampling pipeline [57], the training data is generated from patches of 3D meshes via Poisson disk sampling. Specifically, the training data includes a total of 69,000 samples (patches), where each sample has 256 input points (low resolution) and a corresponding ground-truth of 1,024 points ( $4 \times$  high resolution).
- **PU-GAN Dataset:** This is an earlier dataset that was first used in PU-GAN [28] and generated in a similar way as PU1K but on a smaller scale. To be concrete, the training data comprises 24,000 samples (patches) collected from 120 3D meshes, while the testing data only contains 27 meshes. In addition to the PU1K dataset consisting of a large volume of data targeting the basic  $4 \times$  upsampling experiment, we conduct both  $4 \times$  and  $16 \times$  upsampling experiments based on the compact data of the PU-GAN dataset.

**Evaluation Metrics:** As for the testing process, we follow common practice that has been widely utilized in previous point cloud upsampling works [57, 28, 29, 41]. To

Table 2: Quantitative comparisons to state-of-the-art methods on the *PU-GAN* dataset [28]. (“**CD**”: Chamfer Distance; “**HD**”: Hausdorff Distance; “**P2F**”: Point-to-Surface Distance. All metric units are  $10^{-3}$ , and the best performances are denoted in **bold**.)

| Methods     | 4 $\times$ Upsampling  |                        |                         | 16 $\times$ Upsampling |                        |                         |
|-------------|------------------------|------------------------|-------------------------|------------------------|------------------------|-------------------------|
|             | <b>CD</b> $\downarrow$ | <b>HD</b> $\downarrow$ | <b>P2F</b> $\downarrow$ | <b>CD</b> $\downarrow$ | <b>HD</b> $\downarrow$ | <b>P2F</b> $\downarrow$ |
| PU-Net [58] | 0.844                  | 7.061                  | 9.431                   | 0.699                  | 8.594                  | 11.619                  |
| MPU [57]    | 0.632                  | 6.998                  | 6.199                   | 0.348                  | 7.187                  | 6.822                   |
| PU-GAN [28] | 0.483                  | 5.323                  | 5.053                   | 0.269                  | 7.127                  | 6.306                   |
| Dis-PU [29] | 0.315                  | 4.201                  | 4.149                   | <b>0.199</b>           | 4.716                  | 4.249                   |
| <b>Ours</b> | <b>0.273</b>           | <b>2.605</b>           | <b>1.836</b>            | 0.241                  | <b>2.310</b>           | <b>1.687</b>            |

be specific, at first, we cut the input point cloud into multiple seed patches covering all the  $N$  points. Then, we apply the trained PU-Transformer model to upsample the seed patches with a scale of  $r$ . Finally, the farthest point sampling algorithm [39] is used to combine all the upsampled patches as a dense output point cloud with  $rN$  points. For the  $4 \times$  upsampling experiments in this paper, each testing sample has a low-resolution point cloud with 2,048 points, as well as a high-resolution one with 8,196 points. Coupled with the original 3D meshes, we quantitatively evaluate the upsampling performance of our PU-Transformer based on three widely used metrics: (i) Chamfer Distance (CD), (ii) Hausdorff Distance [6] (HD), and (iii) Point-to-Surface Distance (P2F). A lower value under these metrics denotes better upsampling performance.

### 5.2. Point Cloud Upsampling Results

**PU1K:** Table 1 shows the quantitative results of our PU-Transformer on the PU1K dataset. It can be seen that our approach outperforms other state-of-the-art methods on all three metrics. In terms of the Chamfer Distance metric, we achieve the best performance among all the tested networks, since the reported values of others are all higher than ours of 0.451. Under the other two metrics, the improvements of PU-Transformer are particularly significant: compared to the performance of the recent PU-GCN [41], our approach can almost *halve* the values assessed under both the Hausdorff Distance (HD: 7.577  $\rightarrow$  3.843) and the Point-to-Surface Distance (P2F: 2.499  $\rightarrow$  1.277).

**PU-GAN Dataset:** In addition, we conduct point cloud upsampling experiments using the dataset introduced in PU-GAN [28]. With a smaller scale of training data, we test more upsampling scales in comparison to different networks. To be specific with the results in Table 2, we successfully achieve state-of-the-art performance under all three evaluation metrics for the  $4 \times$  upsampling experiment. However, in the  $16 \times$  upsampling test, we (CD: 0.241) are slightly behind the latest Dis-PU network [29] (CD: 0.199) evaluated under the Chamfer Distance metric: the Dis-PU applies two CD-related items as its loss function, hence getting an edge for CD metric only. As for the results under

Table 3: Ablation study of the PU-Transformer’s components tested on the *PUIK* dataset [41]. Specifically, models  $A_1$ - $A_3$  investigate the effects of the Positional Fusion block, models  $B_1$ - $B_3$  compare the results of different self-attention approaches, and models  $C_1$ - $C_3$  test the upsampling methods in the tail.

| models | PU-Transformer Body    |                | PU-Transformer Tail | Results ( $\times 10^{-3}$ ) |                 |                  |
|--------|------------------------|----------------|---------------------|------------------------------|-----------------|------------------|
|        | Positional Fusion      | Attention Type |                     | CD $\downarrow$              | HD $\downarrow$ | P2F $\downarrow$ |
| $A_1$  | None                   | SC-MSA         | Shuffle             | 0.605                        | 6.477           | 2.038            |
| $A_2$  | $G_{geo}$              | SC-MSA         | Shuffle             | 0.558                        | 5.713           | 1.751            |
| $A_3$  | $G_{feat}$             | SC-MSA         | Shuffle             | 0.497                        | 4.164           | 1.511            |
| $B_1$  | $G_{geo}$ & $G_{feat}$ | SA [54]        | Shuffle             | 0.526                        | 4.689           | 1.492            |
| $B_2$  | $G_{geo}$ & $G_{feat}$ | OSA [17]       | Shuffle             | 0.509                        | 4.823           | 1.586            |
| $B_3$  | $G_{geo}$ & $G_{feat}$ | MSA [52]       | Shuffle             | 0.498                        | 4.218           | 1.427            |
| $C_1$  | $G_{geo}$ & $G_{feat}$ | SC-MSA         | MLPs [58]           | 1.070                        | 8.732           | 2.467            |
| $C_2$  | $G_{geo}$ & $G_{feat}$ | SC-MSA         | DupGrid [57]        | 0.485                        | 3.966           | 1.380            |
| $C_3$  | $G_{geo}$ & $G_{feat}$ | SC-MSA         | NodeShuffle [41]    | 0.505                        | 4.157           | 1.404            |
| Full   | $G_{geo}$ & $G_{feat}$ | SC-MSA         | Shuffle             | <b>0.451</b>                 | <b>3.843</b>    | <b>1.277</b>     |

Hausdorff Distance and Point-to-Surface Distance metrics, our PU-Transformer shows significant improvements again, where some values (e.g., P2F in  $4\times$ , HD and P2F in  $16\times$ ) are even lower than *half* of Dis-PU’s results.

**Overall Comparison:** In general, the experimental results in Table 1 and 2 indicate the great effectiveness of our PU-Transformer. Moreover, by quantitatively comparing to the CNN-based (e.g., GCN [27], GAN [16]) methods under different datasets, we are the first to demonstrate the superiority of a transformer model for point cloud upsampling.

### 5.3. Ablation Studies

**Effects of Components:** Table 3 shows the experiments that replace PU-Transformer’s major components with different options. Specifically, we test three simplified models ( $A_1$ - $A_3$ ) regarding the Positional Encoding block output (Eq. 5), where employing both local *geometric*  $G_{geo}$  and *feature*  $G_{feat}$  context (model “Full”) provides better performance compared to the others. As for models  $B_1$ - $B_3$ , we apply different self-attention approaches to the Transformer Encoder, where our proposed SC-MSA (Sec. 3.3) block shows higher effectiveness on point cloud upsampling. In terms of the upsampling method used in the PU-Transformer tail, some learning-based methods are evaluated as in models  $C_1$ - $C_3$ . Particularly, the shuffle operation [48] indicates an effective and efficient way to obtain a high-resolution feature map since the output of the PU-Transformer body has been sufficiently informative.

**Robustness to Noise:** As the PU-Transformer can upsample different types of point clouds, including real scanned data, it is necessary to verify our model’s robustness to noise. Concretely, we test the pre-trained models by adding some random noise to the sparse input data, where the noise is generated from a standard normal distribution  $\mathcal{N}(0, 1)$  and multiplied with a factor  $\beta$ . In practice, we conduct the experiments under three noise levels:  $\beta = 0.5\%$ ,  $1\%$  and  $2\%$ . Table 4 quantitatively compares the testing results of state-of-the-art methods, and our proposed PU-Transformer achieves the best performance in all tested noise cases.

Table 4: The model’s robustness to random noise tested on the *PUIK* dataset [41]. The noise is generated from the standard normal distribution  $\mathcal{N}(0, 1)$ , and  $\beta$  denotes the noise level.

| Methods     | $\beta = 0.5\%$ |                 |                  | $\beta = 1\%$   |                 |                  | $\beta = 2\%$   |                 |                  |
|-------------|-----------------|-----------------|------------------|-----------------|-----------------|------------------|-----------------|-----------------|------------------|
|             | CD $\downarrow$ | HD $\downarrow$ | P2F $\downarrow$ | CD $\downarrow$ | HD $\downarrow$ | P2F $\downarrow$ | CD $\downarrow$ | HD $\downarrow$ | P2F $\downarrow$ |
| PU-Net [58] | 1.006           | 14.640          | 5.253            | 1.017           | 14.998          | 6.851            | 1.333           | 19.964          | 10.378           |
| MPU [57]    | 0.869           | 12.524          | 4.069            | 0.907           | 13.019          | 5.625            | 1.130           | 16.252          | 9.291            |
| PU-GCN [41] | 0.621           | 8.011           | 3.524            | 0.762           | 9.553           | 5.585            | 1.107           | 13.130          | 9.378            |
| <b>Ours</b> | <b>0.453</b>    | <b>4.052</b>    | <b>2.127</b>     | <b>0.610</b>    | <b>5.787</b>    | <b>3.965</b>     | <b>1.058</b>    | <b>9.948</b>    | <b>7.551</b>     |

Table 5: Model Complexity of PU-Transformer using different numbers of Transformer Encoders. All the experiments are operated on *PUIK* dataset [41] with a single GeForce 2080 Ti GPU.

| # Transformer Encoders | # Parameters | Model Size | Training Speed (per batch) | Inference Speed (per sample) | Results ( $\times 10^{-3}$ ) |                 |                  |
|------------------------|--------------|------------|----------------------------|------------------------------|------------------------------|-----------------|------------------|
|                        |              |            |                            |                              | CD $\downarrow$              | HD $\downarrow$ | P2F $\downarrow$ |
| $L = 3$                | 438.3k       | 8.5M       | 12.2s                      | 6.9ms                        | 0.487                        | 4.081           | 1.362            |
| $L = 4$                | 547.3k       | 11.5M      | 15.9s                      | 8.2ms                        | 0.472                        | 4.010           | 1.284            |
| $L = 5$                | 969.9k       | 18.4M      | 23.5s                      | 9.9ms                        | 0.451                        | <b>3.843</b>    | 1.277            |
| $L = 6$                | 2634.4k      | 39.8M      | 40.3s                      | 11.0ms                       | <b>0.434</b>                 | 3.996           | <b>1.210</b>     |

**Model Complexity:** Generally, our PU-Transformer is a light ( $< 1M$  parameters) transformer model compared to image transformers [24, 31, 14] that usually have more than  $50M$  parameters. In particular, we investigate the complexity of our PU-Transformer by utilizing different numbers of the Transformer Encoders. As shown in Table 5, with more Transformer Encoders being applied, the model complexity increases rapidly, while the quantitative performance improves slowly. For a better balance between effectiveness and efficiency, we adopt the model with *five* Transformer Encoders ( $L = 5$ ) in this work. Overall speaking, the PU-Transformer is a powerful and affordable transformer model for the point cloud upsampling task.

### 5.4. Visualization

**Qualitative Comparisons:** The qualitative results of different point cloud upsampling models are presented in Fig. 4. Since we utilize the self-attention based structure to capture the point-wise dependencies from a global perspective, the PU-Transformer’s output can better illustrate the overall contours of input point clouds producing fewer outliers (as the zoom-in views show). Moreover, based on the comprehensive local context encoded by our Positional Fusion block, the PU-Transformer precisely upsamples the points with a uniform distribution, retaining much structural detail. Accordingly, the reconstructed meshes present more high-fidelity context with fewer artifacts: *e.g.*, the wings of “dragon” in the 2nd row, the head/foot of “human” in the 4th row, and the body of “tiger” in the last row.

**Upsampling Different Input Sizes:** Fig. 5 shows the results of upsampling different sizes of point cloud data using PU-Transformer. Given a relatively low-resolution point cloud (*e.g.*, 256 or 512 input points), our proposed model is still able to generate dense output with high-fidelity context (*e.g.*, the head/foot of “Panda”). As the input size increases, the new points are uniformly distributed, covering the main flat areas (*e.g.*, the body of “Panda”).

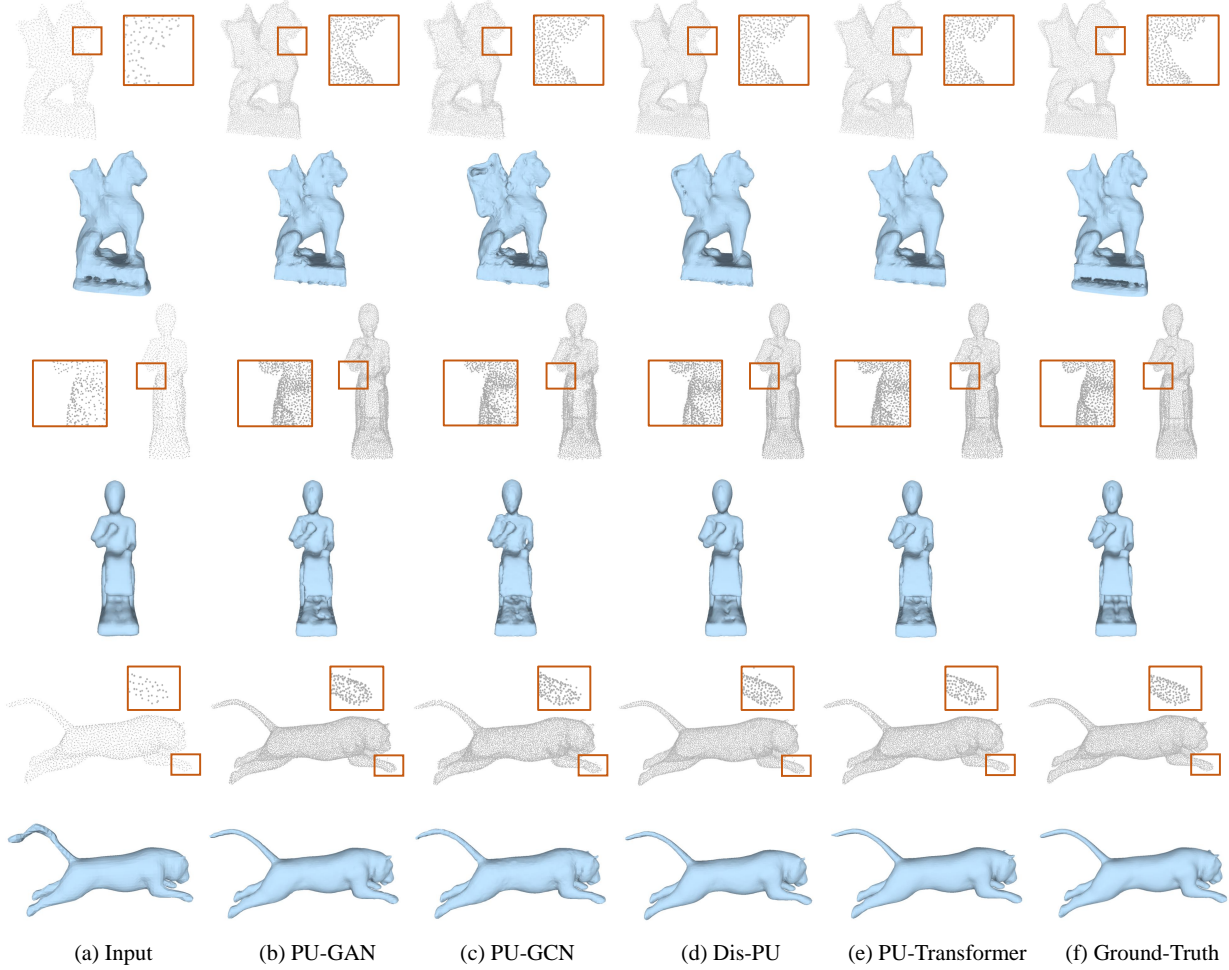


Figure 4: Comparisons to state-of-the-art methods (PU-GAN [28], PU-GCN [41], Dis-PU [29]) in  $4\times$  upsampling experiments using 2048 input points. For a better visualization, we reconstruct the surfaces (in blue) of each point cloud following the algorithm in [23].

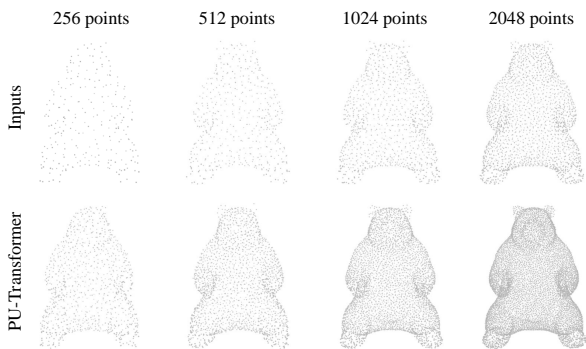


Figure 5: PU-Transformer’s  $4\times$  upsampling results, given different sizes of input point cloud data.

**Upsampling Real Point Clouds:** We also provide the PU-Transformer’s  $4\times$  and  $16\times$  upsampling results on real point cloud samples from *ScanObjectNN* [51], *S3DIS* [3], *ScanNet* [12], and *SemanticKITTI* [5] datasets. As Fig. 1 clearly illustrates, by addressing the sparsity and non-uniformity of

raw inputs, not only is the overall quality of point clouds significantly improved, but also the representative features of object instances are enhanced.

## 6. Conclusions

This paper focuses on low-level vision for point cloud data in order to tackle its inherent *sparsity* and *irregularity*. Specifically, we propose a novel transformer-based model, PU-Transformer, targeting the fundamental point cloud upsampling task. Our PU-Transformer shows significant quantitative and qualitative improvements on different point cloud datasets compared to state-of-the-art CNN-based methods. By conducting related ablation studies and visualizations, we also analyze the effects and robustness of our approach. Given the great potential of PU-Transformer in solving the low-level upsampling problem, in the future, we expect to further optimize its efficiency for real-time applications and extend its adaptability in high-level 3D visual tasks such as semantic segmentation and object detection.

## References

- [1] Martín Abadi, Paul Barham, Jianmin Chen, Zhifeng Chen, Andy Davis, Jeffrey Dean, Matthieu Devin, Sanjay Ghemawat, Geoffrey Irving, Michael Isard, et al. Tensorflow: A system for large-scale machine learning. In *12th {USENIX} symposium on operating systems design and implementation ({OSDI} 16)*, pages 265–283, 2016. 6
- [2] Saeed Anwar, Salman Khan, and Nick Barnes. A deep journey into super-resolution: A survey. *ACM Computing Surveys (CSUR)*, 53(3):1–34, 2020. 1
- [3] Iro Armeni, Sasha Sax, Amir R Zamir, and Silvio Savarese. Joint 2d-3d-semantic data for indoor scene understanding. *arXiv preprint arXiv:1702.01105*, 2017. 1, 8, 13, 15
- [4] Jimmy Lei Ba, Jamie Ryan Kiros, and Geoffrey E Hinton. Layer normalization. *arXiv preprint arXiv:1607.06450*, 2016. 3, 12, 13
- [5] Jens Behley, Martin Garbade, Andres Milioto, Jan Quenzel, Sven Behnke, Cyrill Stachniss, and Jürgen Gall. Semantickitti: A dataset for semantic scene understanding of lidar sequences. In *Proceedings of the IEEE International Conference on Computer Vision*, pages 9297–9307, 2019. 1, 8, 13, 15
- [6] Matthew Berger, Joshua A Levine, Luis Gustavo Nonato, Gabriel Taubin, and Claudio T Silva. A benchmark for surface reconstruction. *ACM Transactions on Graphics (TOG)*, 32(2):1–17, 2013. 6
- [7] Holger Caesar, Varun Bankiti, Alex H Lang, Sourabh Vora, Venice Erin Liang, Qiang Xu, Anush Krishnan, Yu Pan, Giacarlo Baldan, and Oscar Beijbom. nuscenes: A multi-modal dataset for autonomous driving. In *Proceedings of the IEEE/CVF conference on computer vision and pattern recognition*, pages 11621–11631, 2020. 1
- [8] Nicolas Carion, Francisco Massa, Gabriel Synnaeve, Nicolas Usunier, Alexander Kirillov, and Sergey Zagoruyko. End-to-end object detection with transformers. In *European Conference on Computer Vision*, pages 213–229. Springer, 2020. 2, 3
- [9] Angel X Chang, Thomas Funkhouser, Leonidas Guibas, Pat Hanrahan, Qixing Huang, Zimo Li, Silvio Savarese, Manolis Savva, Shuran Song, Hao Su, et al. Shapenet: An information-rich 3d model repository. *arXiv preprint arXiv:1512.03012*, 2015. 6
- [10] Hanting Chen, Yunhe Wang, Tianyu Guo, Chang Xu, Yiping Deng, Zhenhua Liu, Siwei Ma, Chunjing Xu, Chao Xu, and Wen Gao. Pre-trained image processing transformer. In *Proceedings of the IEEE/CVF Conference on Computer Vision and Pattern Recognition*, pages 12299–12310, 2021. 2, 3
- [11] Christopher Choy, JunYoung Gwak, and Silvio Savarese. 4d spatio-temporal convnets: Minkowski convolutional neural networks. In *Proceedings of the IEEE/CVF Conference on Computer Vision and Pattern Recognition*, pages 3075–3084, 2019. 3
- [12] Angela Dai, Angel X Chang, Manolis Savva, Maciej Halber, Thomas Funkhouser, and Matthias Nießner. Scannet: Richly-annotated 3d reconstructions of indoor scenes. In *Proceedings of the IEEE conference on computer vision and pattern recognition*, pages 5828–5839, 2017. 1, 8, 13, 15
- [13] Chao Dong, Chen Change Loy, Kaiming He, and Xiaoou Tang. Image super-resolution using deep convolutional networks. *IEEE transactions on pattern analysis and machine intelligence*, 38(2):295–307, 2015. 1
- [14] Alexey Dosovitskiy, Lucas Beyer, Alexander Kolesnikov, Dirk Weissenborn, Xiaohua Zhai, Thomas Unterthiner, Mostafa Dehghani, Matthias Minderer, Georg Heigold, Sylvain Gelly, et al. An image is worth 16x16 words: Transformers for image recognition at scale. *arXiv preprint arXiv:2010.11929*, 2020. 2, 3, 7
- [15] Felix Endres, Jürgen Hess, Jürgen Sturm, Daniel Cremers, and Wolfram Burgard. 3-d mapping with an rgb-d camera. *IEEE transactions on robotics*, 30(1):177–187, 2013. 1
- [16] Ian Goodfellow, Jean Pouget-Abadie, Mehdi Mirza, Bing Xu, David Warde-Farley, Sherjil Ozair, Aaron Courville, and Yoshua Bengio. Generative adversarial nets. *Advances in neural information processing systems*, 27, 2014. 3, 7
- [17] Meng-Hao Guo, Jun-Xiong Cai, Zheng-Ning Liu, Tai-Jiang Mu, Ralph R Martin, and Shi-Min Hu. Pct: Point cloud transformer. *Computational Visual Media*, 7(2):187–199, 2021. 3, 7
- [18] Yulan Guo, Hanyun Wang, Qingyong Hu, Hao Liu, Li Liu, and Mohammed Bennamoun. Deep learning for 3d point clouds: A survey. *IEEE transactions on pattern analysis and machine intelligence*, 2020. 3
- [19] Qingyong Hu, Bo Yang, Linhai Xie, Stefano Rosa, Yulan Guo, Zhihua Wang, Niki Trigoni, and Andrew Markham. Randla-net: Efficient semantic segmentation of large-scale point clouds. In *Proceedings of the IEEE/CVF Conference on Computer Vision and Pattern Recognition*, pages 11108–11117, 2020. 1, 3
- [20] Jing Huang and Suya You. Point cloud labeling using 3d convolutional neural network. In *2016 23rd International Conference on Pattern Recognition (ICPR)*, pages 2670–2675. IEEE, 2016. 3
- [21] Sergey Ioffe and Christian Szegedy. Batch normalization: Accelerating deep network training by reducing internal covariate shift. *arXiv preprint arXiv:1502.03167*, 2015. 5, 12, 13
- [22] Michel Jaboyedoff, Thierry Oppikofer, Antonio Abellán, Marc-Henri Derron, Alex Loyer, Richard Metzger, and Andrea Pedrazzini. Use of lidar in landslide investigations: a review. *Natural hazards*, 61(1):5–28, 2012. 1
- [23] Michael Kazhdan and Hugues Hoppe. Screened poisson surface reconstruction. *ACM Transactions on Graphics (ToG)*, 32(3):1–13, 2013. 8
- [24] Salman Khan, Muzammal Naseer, Munawar Hayat, Syed Waqas Zamir, Fahad Shahbaz Khan, and Mubarak Shah. Transformers in vision: A survey. *arXiv preprint arXiv:2101.01169*, 2021. 3, 7
- [25] Jiwon Kim, Jung Kwon Lee, and Kyoung Mu Lee. Accurate image super-resolution using very deep convolutional networks. In *Proceedings of the IEEE conference on computer vision and pattern recognition*, pages 1646–1654, 2016. 1
- [26] Felix Järemo Lawin, Martin Danelljan, Patrik Tosteberg, Goutam Bhat, Fahad Shahbaz Khan, and Michael Felsberg. Deep projective 3d semantic segmentation. In *International*

*Conference on Computer Analysis of Images and Patterns*, pages 95–107. Springer, 2017. 3

[27] Guohao Li, Matthias Muller, Ali Thabet, and Bernard Ghanem. Deepgcns: Can gcns go as deep as cnns? In *Proceedings of the IEEE/CVF International Conference on Computer Vision*, pages 9267–9276, 2019. 7

[28] Ruihui Li, Xianzhi Li, Chi-Wing Fu, Daniel Cohen-Or, and Pheng-Ann Heng. Pu-gan: a point cloud upsampling adversarial network. In *Proceedings of the IEEE International Conference on Computer Vision*, pages 7203–7212, 2019. 1, 3, 4, 6, 8, 12, 13

[29] Ruihui Li, Xianzhi Li, Pheng-Ann Heng, and Chi-Wing Fu. Point cloud upsampling via disentangled refinement. In *Proceedings of the IEEE/CVF Conference on Computer Vision and Pattern Recognition*, pages 344–353, 2021. 1, 2, 3, 6, 8, 12, 13

[30] Yongcheng Liu, Bin Fan, Shiming Xiang, and Chunhong Pan. Relation-shape convolutional neural network for point cloud analysis. In *Proceedings of the IEEE Conference on Computer Vision and Pattern Recognition*, pages 8895–8904, 2019. 1

[31] Ze Liu, Yutong Lin, Yue Cao, Han Hu, Yixuan Wei, Zheng Zhang, Stephen Lin, and Baining Guo. Swin transformer: Hierarchical vision transformer using shifted windows. In *Proceedings of the IEEE/CVF International Conference on Computer Vision (ICCV)*, pages 10012–10022, October 2021. 2, 3, 7

[32] Kirill Mazur and Victor Lempitsky. Cloud transformers: A universal approach to point cloud processing tasks. In *Proceedings of the IEEE/CVF International Conference on Computer Vision*, pages 10715–10724, 2021. 3

[33] Niloy J Mitra, Natasha Gelfand, Helmut Pottmann, and Leonidas Guibas. Registration of point cloud data from a geometric optimization perspective. In *Proceedings of the 2004 Eurographics/ACM SIGGRAPH symposium on Geometry processing*, pages 22–31. ACM, 2004. 1

[34] Niloy J Mitra and An Nguyen. Estimating surface normals in noisy point cloud data. In *Proceedings of the nineteenth annual symposium on Computational geometry*, pages 322–328. ACM, 2003. 1

[35] Vinod Nair and Geoffrey E Hinton. Rectified linear units improve restricted boltzmann machines. In *Icml*, 2010. 5

[36] Dennis Park, Rares Ambrus, Vitor Guizilini, Jie Li, and Adrien Gaidon. Is pseudo-lidar needed for monocular 3d object detection? In *Proceedings of the IEEE/CVF International Conference on Computer Vision (ICCV)*, pages 3142–3152, October 2021. 1

[37] Charles R Qi, Xinlei Chen, Or Litany, and Leonidas J Guibas. Imvotenet: Boosting 3d object detection in point clouds with image votes. In *Proceedings of the IEEE/CVF conference on computer vision and pattern recognition*, pages 4404–4413, 2020. 1

[38] Charles R Qi, Or Litany, Kaiming He, and Leonidas J Guibas. Deep hough voting for 3d object detection in point clouds. In *Proceedings of the IEEE/CVF International Conference on Computer Vision*, pages 9277–9286, 2019. 1, 3, 13

[39] Charles R Qi, Hao Su, Kaichun Mo, and Leonidas J Guibas. Pointnet: Deep learning on point sets for 3d classification and segmentation. In *Proceedings of the IEEE Conference on Computer Vision and Pattern Recognition*, pages 652–660, 2017. 1, 3, 6, 13

[40] Charles Ruizhongtai Qi, Li Yi, Hao Su, and Leonidas J Guibas. Pointnet++: Deep hierarchical feature learning on point sets in a metric space. In *Advances in neural information processing systems*, pages 5099–5108, 2017. 1, 3

[41] Guocheng Qian, Abdulellah Abualshour, Guohao Li, Ali Thabet, and Bernard Ghanem. Pu-gcn: Point cloud upsampling using graph convolutional networks. In *Proceedings of the IEEE/CVF Conference on Computer Vision and Pattern Recognition*, pages 11683–11692, 2021. 1, 3, 4, 5, 6, 7, 8, 12, 13

[42] Yue Qian, Junhui Hou, Sam Kwong, and Ying He. Pugeonet: A geometry-centric network for 3d point cloud upsampling. In *European Conference on Computer Vision*, pages 752–769. Springer, 2020. 1, 3, 4, 12, 13

[43] Shi Qiu, Saeed Anwar, and Nick Barnes. Dense-resolution network for point cloud classification and segmentation. In *Proceedings of the IEEE/CVF Winter Conference on Applications of Computer Vision (WACV)*, pages 3813–3822, January 2021. 1

[44] Shi Qiu, Saeed Anwar, and Nick Barnes. Geometric back-projection network for point cloud classification. *IEEE Transactions on Multimedia*, 2021. 1, 2

[45] Shi Qiu, Saeed Anwar, and Nick Barnes. Pnp-3d: A plug-and-play for 3d point clouds. *arXiv preprint arXiv:2108.07378*, 2021. 1, 12

[46] Shi Qiu, Saeed Anwar, and Nick Barnes. Semantic segmentation for real point cloud scenes via bilateral augmentation and adaptive fusion. In *Proceedings of the IEEE/CVF Conference on Computer Vision and Pattern Recognition (CVPR)*, pages 1757–1767, 2021. 1

[47] Shi Qiu, Yunfan Wu, Saeed Anwar, and Chongyi Li. Investigating attention mechanism in 3d point cloud object detection. In *International Conference on 3D Vision (3DV)*. IEEE, 2021. 1, 2

[48] Wenzhe Shi, Jose Caballero, Ferenc Huszár, Johannes Totz, Andrew P Aitken, Rob Bishop, Daniel Rueckert, and Zehan Wang. Real-time single image and video super-resolution using an efficient sub-pixel convolutional neural network. In *Proceedings of the IEEE conference on computer vision and pattern recognition*, pages 1874–1883, 2016. 3, 5, 7

[49] Hang Su, Varun Jampani, Deqing Sun, Subhransu Maji, Evangelos Kalogerakis, Ming-Hsuan Yang, and Jan Kautz. Splatnet: Sparse lattice networks for point cloud processing. In *Proceedings of the IEEE Conference on Computer Vision and Pattern Recognition*, pages 2530–2539, 2018. 3

[50] Hang Su, Subhransu Maji, Evangelos Kalogerakis, and Erik Learned-Miller. Multi-view convolutional neural networks for 3d shape recognition. In *Proceedings of the IEEE international conference on computer vision*, pages 945–953, 2015. 3

[51] Mikaela Angelina Uy, Quang-Hieu Pham, Binh-Son Hua, Thanh Nguyen, and Sai-Kit Yeung. Revisiting point cloud

classification: A new benchmark dataset and classification model on real-world data. In *Proceedings of the IEEE/CVF International Conference on Computer Vision*, pages 1588–1597, 2019. 1, 8, 13, 15

[52] Ashish Vaswani, Noam Shazeer, Niki Parmar, Jakob Uszkoreit, Llion Jones, Aidan N Gomez, Łukasz Kaiser, and Illia Polosukhin. Attention is all you need. In *Advances in neural information processing systems*, pages 5998–6008, 2017. 2, 3, 4, 5, 7, 12

[53] Qilong Wang, Banggu Wu, Pengfei Zhu, Peihua Li, Wangmeng Zuo, and Qinghua Hu. Eca-net: Efficient channel attention for deep convolutional neural networks. In *IEEE/CVF Conference on Computer Vision and Pattern Recognition (CVPR)*, June 2020. 5

[54] Xiaolong Wang, Ross Girshick, Abhinav Gupta, and Kaiming He. Non-local neural networks. In *Proceedings of the IEEE Conference on Computer Vision and Pattern Recognition*, pages 7794–7803, 2018. 5, 7

[55] Yue Wang, Yongbin Sun, Ziwei Liu, Sanjay E Sarma, Michael M Bronstein, and Justin M Solomon. Dynamic graph cnn for learning on point clouds. *ACM Transactions on Graphics (TOG)*, 38(5):146, 2019. 1, 3, 4, 5

[56] Fuzhi Yang, Huan Yang, Jianlong Fu, Hongtao Lu, and Baineng Guo. Learning texture transformer network for image super-resolution. In *Proceedings of the IEEE/CVF Conference on Computer Vision and Pattern Recognition*, pages 5791–5800, 2020. 3

[57] Wang Yifan, Shihao Wu, Hui Huang, Daniel Cohen-Or, and Olga Sorkine-Hornung. Patch-based progressive 3d point set upsampling. In *Proceedings of the IEEE/CVF Conference on Computer Vision and Pattern Recognition*, pages 5958–5967, 2019. 1, 2, 3, 4, 6, 7, 12, 13

[58] Lequan Yu, Xianzhi Li, Chi-Wing Fu, Daniel Cohen-Or, and Pheng-Ann Heng. Pu-net: Point cloud upsampling network. In *Proceedings of the IEEE Conference on Computer Vision and Pattern Recognition*, pages 2790–2799, 2018. 1, 2, 3, 4, 6, 7, 12, 13

[59] Xumin Yu, Yongming Rao, Ziyi Wang, Zuyan Liu, Jiwen Lu, and Jie Zhou. Pointr: Diverse point cloud completion with geometry-aware transformers. In *Proceedings of the IEEE/CVF International Conference on Computer Vision*, pages 12498–12507, 2021. 3

[60] Wentao Yuan, Tejas Khot, David Held, Christoph Mertz, and Martial Hebert. Pcn: Point completion network. In *2018 International Conference on 3D Vision (3DV)*, pages 728–737. IEEE, 2018. 3

[61] Hengshuang Zhao, Li Jiang, Jiaya Jia, Philip HS Torr, and Vladlen Koltun. Point transformer. In *Proceedings of the IEEE/CVF International Conference on Computer Vision*, pages 16259–16268, 2021. 2, 3

[62] Xizhou Zhu, Weijie Su, Lewei Lu, Bin Li, Xiaogang Wang, and Jifeng Dai. Deformable detr: Deformable transformers for end-to-end object detection. *arXiv preprint arXiv:2010.04159*, 2020. 3

# Supplementary Material

## A. Overview

This supplementary material includes behavior analysis, ablation studies, limitations, visualizations, and future direction of our PU-Transformer for point cloud upsampling.

## B. Behavior Analysis

**Positional Fusion Block:** Although our Positional Fusion block utilizes similar operations as the Local Context Fusion (LCF) block proposed in [45], there are three main differences between these two methods. First, our block operates on the *patches* of point clouds that have explicit borders, while the LCF extracts the local context from a *whole* point cloud where more outliers could be involved. Second, all of our blocks in PU-Transformer share the *same* geometric relations, but each LCF block requires a *distinct* geometric relation that is specified in the corresponding point cloud resolution. Last but not least, our block serves as a feature *encoding* block that helps to gradually expand the channel dimension of the point cloud feature map, while the LCF aims to *refine* the feature representations in the same embedding space of the input. In addition, the effects of our Positional Fusion block can be analyzed from the comparisons in Figure 6: by applying the block, the generated points can better align with the contour of a point cloud object, retaining high-fidelity local detail with fewer outliers.

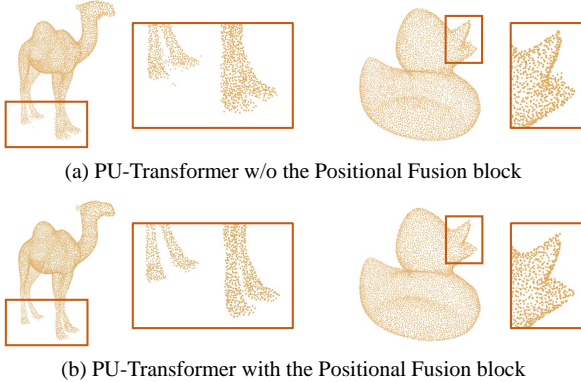


Figure 6: Upsampling results of the PU-Transformer *with* and *without* using the Positional Fusion block.

**SC-MSA Block:** In Sec. 3.3 of the main paper, we state that it is easier for our SC-MSA block to integrate the information between the connected multi-head outputs compared to regular MSA [52]. The main reason can be explained as follows: since two consecutive heads share some input channels, both of the two heads' outputs are affected/regulated by such shared channel-wise information, leading to less varying estimations of point-wise dependencies. As *any* two consecutive heads in our SC-MSA will

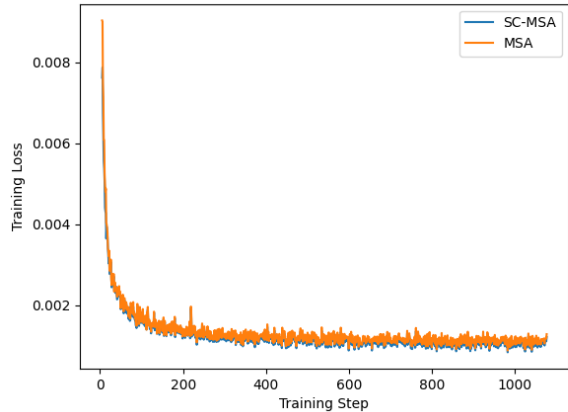


Figure 7: The training loss of using SC-MSA or MSA [52] in the PU-Transformer body, respectively. Overall, compared to regular MSA block, our SC-MSA contributes to a better convergence (lower loss) in the training procedure.

follow the above manner, the outputs of all connected multi-heads become less varying, benefiting the overall estimations of point-wise dependencies. Moreover, there is practical evidence to support it: as shown in Figure 7, we clearly observe that the overall training loss of using SC-MSA is lower than using MSA. In other words, by using the SC-MSA, the integrated information can help our upsampling predictions better approach the given dense ground-truths.

## C. Ablation Studies

**Normalization Operations:** As indicated in Fig. 2 and Alg. 1 of the main paper, the Transformer Encoder incorporates two normalization operations in the fashion of transformers. In practice, NLP-related models favor layer normalization (LN) [4] while image-related methods prefer batch normalization (BN) [21]. In terms of the point cloud upsampling task, we select the type of normalization operations (*i.e.*, “Norm<sub>1</sub>” and “Norm<sub>2</sub>” in Table 6) in the PU-Transformer based on the practical performance. Table 6 shows the quantitative results of *five* options ( $D_1$  to  $D_5$ ), indicating that the two normalization operations are crucial while the effects of BN and LN are very similar. Considering the relative simplicity and effectiveness, we thus adopt the LN operation for both “Norm<sub>1</sub>” and “Norm<sub>2</sub>” (*i.e.*, model  $D_5$ ), in order to further regulate the point features encoded by our Positional Fusion and SC-MSA blocks.

**PU1K and PU-GAN Datasets:** Different from some works [58, 57, 42] testing their proposed models using their own data, we quantitatively evaluate the PU-Transformer on two public datasets: PU1K [41] and PU-GAN [28]. Particularly, we utilize the same experimental settings and results from PU-GCN [41] and Dis-PU [29], in order to have a fair comparison with state-of-the-art methods in Tab. 1 and 2 of

Table 6: PU-Transformer’s quantitative results of using different normalization operations in the Transformer Encoder, tested on the *PUIK* dataset [41]. The best results are denoted in **bold**. (“Norm<sub>1</sub>”: the operation applied in step 4 of Alg. 1; “Norm<sub>2</sub>”: the operation applied in step 5 of Alg. 1; “BN”: batch normalization [21]; “LN”: layer normalization [4]; “CD”: Chamfer Distance; “HD”: Hausdorff Distance; “P2F”: Point-to-Surface Distance.)

| models                | Norm <sub>1</sub> | Norm <sub>2</sub> | CD <sub>↓</sub><br>( $\times 10^{-3}$ ) | HD <sub>↓</sub><br>( $\times 10^{-3}$ ) | P2F <sub>↓</sub><br>( $\times 10^{-3}$ ) |
|-----------------------|-------------------|-------------------|---|---|--|
| <i>D</i> <sub>1</sub> | <i>none</i>       | <i>none</i>       | 0.684                                   | 6.810                                   | 1.522                                    |
| <i>D</i> <sub>2</sub> | BN                | BN                | 0.453                                   | 4.144                                   | 1.395                                    |
| <i>D</i> <sub>3</sub> | BN                | LN                | <b>0.441</b>                            | 3.869                                   | 1.306                                    |
| <i>D</i> <sub>4</sub> | LN                | BN                | 0.477                                   | 4.105                                   | 1.285                                    |
| <i>D</i> <sub>5</sub> | LN                | LN                | 0.451                                   | <b>3.843</b>                            | <b>1.277</b>                             |

the main paper. Moreover, we investigate the difference between the *PUIK* and *PU-GAN* datasets by *swapping* their training and testing data. According to the results (*E*<sub>1</sub>&*E*<sub>2</sub>, *E*<sub>3</sub>&*E*<sub>4</sub>) in Table 7, we find that given a small scale of training data<sup>4</sup>, our PU-Transformer can still achieve a similar performance when using a large scale of training data<sup>5</sup>. In addition, as shown between *E*<sub>1</sub>&*E*<sub>3</sub> or *E*<sub>2</sub>&*E*<sub>4</sub>, the test set of *PUIK* is more challenging than the *PU-GAN*’s, since there are 100 more testing samples in the *PUIK* dataset.

## D. Limitations

**Model Efficiency:** As mentioned in the main paper, regular transformer models emphasize the effectiveness of visual applications, while the efficiency is not comparable to the CNN-based counterparts. Although PU-Transformer is a light transformer model, in point cloud upsampling, it still consumes more trainable parameters than some CNN-based methods [58, 38, 41, 29], producing a larger model as indicated in Table 8. For the inference in practice, the speed of our approach is very close to others due to the fast parallel computing capability of GPUs. In contrast, the networks that apply complex architectures [28, 29] or conduct expensive geometric calculations [42] will be a bit slower.

**Upsampling Flexibility:** Since our approach follows a supervised end-to-end training paradigm, by conducting a single iteration of inference, we can only obtain the upsampling results in a fixed scale (*i.e.*, upsampling ratio  $r$ ). To generate other resolutions of outputs using a pre-trained PU-Transformer model, we have to apply some post-processing such as the farthest point sampling algorithm [39] and multiple iterations of inference. For further improvement, we consider keeping the PU-Transformer’s head and body for point feature encoding but designing a more flexible tail to generate different resolutions of outputs. The code and pre-trained models of PU-Transformer will be available at <https://github.com/>.

<sup>4</sup>24,000 samples in the *PU-GAN* dataset

<sup>5</sup>69,000 samples in the *PUIK* dataset

Table 7: PU-Transformer’s quantitative results when using different training and testing data from *PUIK* dataset [41] and *PU-GAN* dataset [28]. (“CD”: Chamfer Distance; “HD”: Hausdorff Distance; “P2F”: Point-to-Surface Distance.)

| models                | training data | testing data  | CD <sub>↓</sub><br>( $\times 10^{-3}$ ) | HD <sub>↓</sub><br>( $\times 10^{-3}$ ) | P2F <sub>↓</sub><br>( $\times 10^{-3}$ ) |
|-----------------------|---------------|---------------|---|---|--|
| <i>E</i> <sub>1</sub> | <i>PUIK</i>   | <i>PUIK</i>   | 0.451                                   | 3.843                                   | 1.277                                    |
| <i>E</i> <sub>2</sub> | <i>PU-GAN</i> | <i>PUIK</i>   | 0.469                                   | 4.227                                   | 1.387                                    |
| <i>E</i> <sub>3</sub> | <i>PUIK</i>   | <i>PU-GAN</i> | 0.278                                   | 2.091                                   | 1.838                                    |
| <i>E</i> <sub>4</sub> | <i>PU-GAN</i> | <i>PU-GAN</i> | 0.273                                   | 2.605                                   | 1.836                                    |

Table 8: Efficiency of the point cloud upsampling methods.

| Methods         | PU-Net [58] | MPU [57] | PU-GAN [28] | PUGeo [42] | PU-GCN [41] | Dis-PU [29] | PU-Transformer (ours) |
|-----------------|-------------|----------|-------------|------------|-------------|-------------|-----------------------|
| Inference Speed | 8.4ms       | 8.3ms    | 10.5ms      | –          | 8.0ms       | 10.8ms      | 9.9ms                 |
| Model Size      | 10.1M       | 6.2M     | 9.6M        | 22.9M      | 1.8M        | 13.2M       | 18.4M                 |

## E. Visualizations

**Upsampling Noisy Input:** In Tab. 4 of the main paper, we quantitatively compare the PU-Transformer’s robustness to random noise against other point cloud upsampling methods. Moreover, in Figure 8, we qualitatively visualize its upsampling results under different noise levels. Generally, our approach is robust to random noise since the upsampling results in all noisy cases retain the high-fidelity shapes. However, it is worth noting that the generated point cloud’s uniformity can be affected as the noise level increases.

**Upsampling Different Input Sizes:** In Figure 9, we provide more examples to visualize our PU-Transformer’s performance on upsampling various sizes of point cloud data. Similar to the effects shown in Fig. 5 of the main paper, given different numbers of input points, our proposed model can always generate dense output of high-quality.

**Upsampling Real Point Clouds:** We present a few examples of upsampling real point cloud data with our PU-Transformer. Particularly, Figure 10 illustrates the upsampled results of a LiDAR street [5], an indoor living room [12], a conference room [3], and some real-scanned objects [51]. In general, the overall quality of input data is significantly improved, where the generated points are well organized in a uniform distribution. For object instances (*e.g.*, “cars”, and “chairs”), the representative features have been enhanced, benefiting an easier visual recognition.

## F. Future Direction

As the first transformer model for point cloud upsampling, we believe our PU-Transformer has great potential for different applications. In the low-level vision area, we can propose a *multifunctional* tail targeting multiple tasks, including upsampling, completion, denoising, *etc.* For high-level vision applications, we can develop a lightweight transformer based on the compact structure of the PU-Transformer’s body.

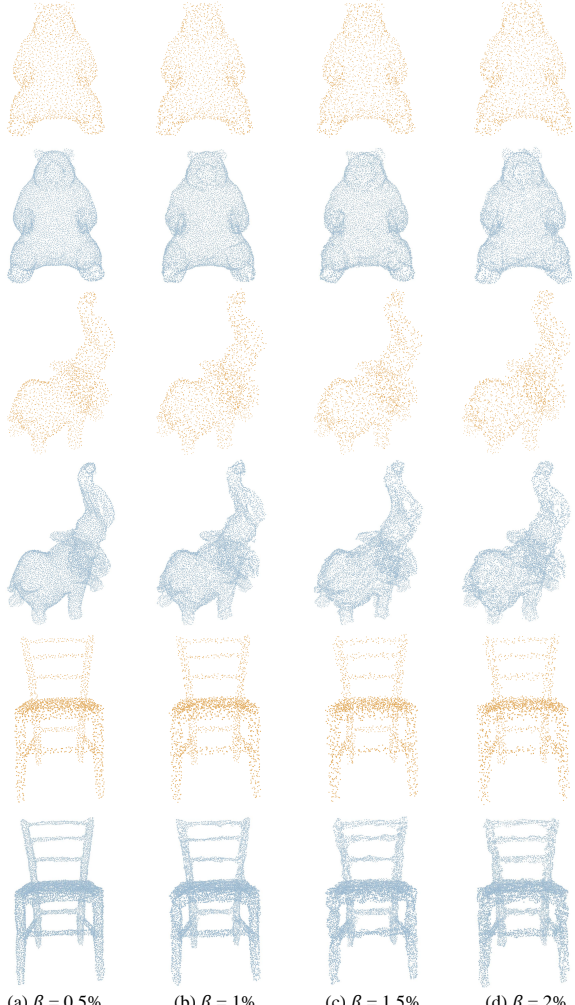


Figure 8: Visualizations of PU-Transformer in upsampling noisy input point clouds, where the noise is generated from a standard normal distribution  $\mathcal{N}(0, 1)$  and multiplied with a factor  $\beta = 0.5\%, 1\%, 1.5\%, \text{ and } 2\%$ , respectively. The input point clouds are in orange color, while the corresponding upsampled results are in blue.

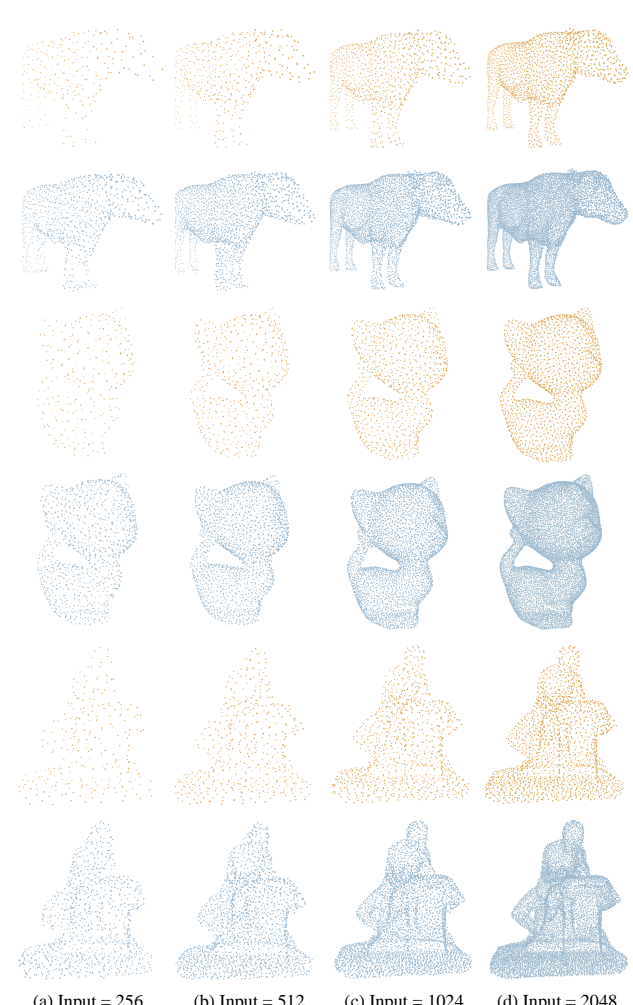


Figure 9: Visualizations of PU-Transformer in upsampling different sizes of point clouds, where the number of input points is 256, 512, 1024, and 2048, respectively. The input point clouds are in orange color, while the corresponding upsampled results are in blue.

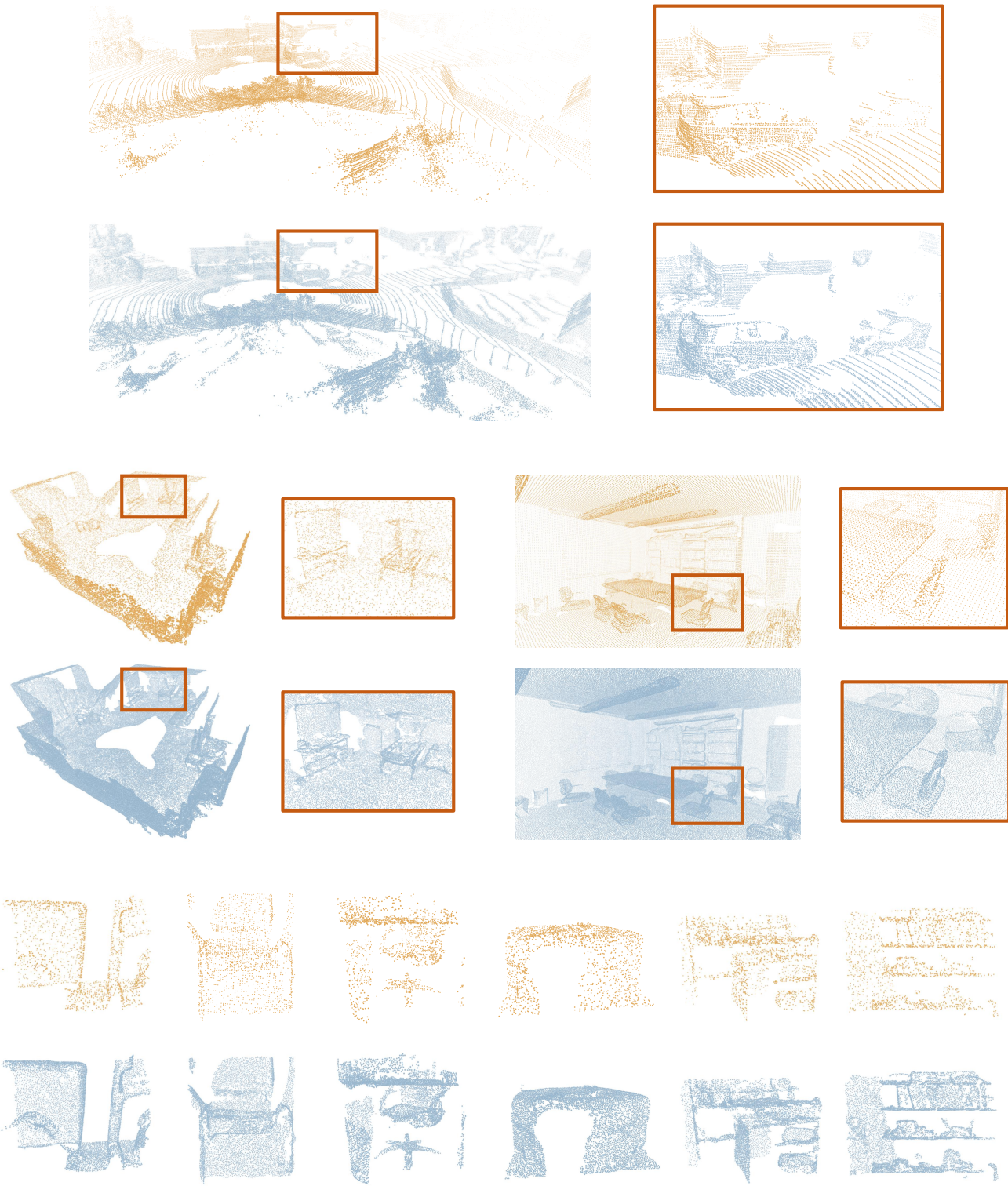


Figure 10: Visualizations of PU-Transformer in upsampling real point clouds, including a LiDAR street (from SemanticKTTI dataset [5]), a living room (from ScanNet dataset [12]), a conference room (from S3DIS dataset [3]), as well as some real-scanned objects (from ScanObjectNN dataset [51]). The input point clouds are in orange color, while the corresponding upsampled results are in blue.